# $N$-body simulation of early structure formation from cosmic string loops

Hao Jiao,[1,*] Robert Brandenberger,[1,†] and Alexandre Refregier[2,‡]
[1]Department of Physics, McGill University, Montréal, Quebec H3A 2T8, Canada
[2]Institute for Particle Physics and Astrophysics, ETH,
Wolfgang-Pauli-Strasse 27, CH-8093 Zurich, Switzerland

(Received 18 March 2024; accepted 17 May 2024; published 14 June 2024)

By means of $N$-body simulations, we study early structure formation in the presence of a scaling distribution of cosmic string loops. Cosmic string loops dominate the high redshift halo mass function while the fluctuations seeded by the standard structure formation scenario dominate structure at low redshifts. In our study, the effects of the cosmic string loops are taken into account by displacing the dark matter particles and their velocities at the initial time of the simulation by amounts determined by the analytical analysis which makes use of the Zel'dovich approximation. We find that the resulting halo mass function is to a good approximation given by the sum of the analytically determined cosmic string halo mass function and the halo mass function obtained from the standard ΛCDM model.

DOI: 10.1103/PhysRevD.109.123524

## I. INTRODUCTION

A subset of particle physics models beyond the Standard Model have solutions corresponding to cosmic string defects (see, e.g., [1–3] for reviews of cosmic strings and their role in early universe cosmology). If Nature is described by such a model, then causality arguments [4] imply that a network of cosmic strings will form in the early universe and persist to the present time. Cosmic strings correspond to lines of trapped energy, and the induced gravitational effects lead to signatures in cosmology. The gravitational effects of strings depend on only one free parameter, namely the string tension $\mu$ which is of the order $\eta^2$, where $\eta$ is the energy scale of the phase transition which leads to defect formation. Searching for the signals of cosmic strings in the sky is hence a way to probe particle physics "from top down" (since the effects are larger for larger values of $\eta$), while usual accelerator searches probe new physics "from bottom up" (since they are more sensitive to physics at lower values of $\eta$).

After the phase transition during which strings form, the distribution of strings rapidly approaches a "scaling solution" [4] according to which the statistical properties of the string distribution are invariant in time $t$ if all lengths are scaled to the Hubble radius $t$.[1] The string network consists of a random-walk-like network of "long strings" (strings with curvature radius comparable to or larger than $t$) and a distribution of string loops which result from the intercommutation of long strings. While the scaling distribution of long strings is robust since it is derived from general causality arguments, the distribution of string loops is less certain since it depends on the decay channels of string loops. It is generally believed that gravitational radiation [5] dominates the loop decay, but some field theory simulations indicate that particle emission might have a large effect [6]. In this paper we shall work in the context of the Nambu-Goto cosmic strings and the "one-scale model" of the distribution of string loops [7] which is supported by the numerical simulations of [8]. According to this model, at any given time $t$ there are string loops with radii $R$ in the range $\gamma G\mu t < R < \alpha t$, where the constant $\alpha$ indicates the mean loop radius $R = \alpha t$ at the time $t$ when the loop is formed, and $\gamma \sim 10^2$ is a constant determined by the strength of gravitational radiation from loop oscillations. The number density in comoving coordinates $n(R,t)dR$ of loops in the radius interval between $R$ and $R + dR$ is (for times after the time of matter and radiation equality, $t_{eq}$) is given by

$$n(R,t) = N\alpha^2\beta^{-2}t_0^{-2}R^{-2} \tag{1}$$

for $\alpha t_{eq} \leq R \leq \alpha t$, and

$$n(R,t) = N\alpha^{5/2}\beta^{-5/2}t_{eq}^{1/2}t_0^{-2}R^{-5/2} \tag{2}$$

for $\gamma G\mu t < R < \alpha t_{eq}$, where $N$ is a constant determined by the number of long strings per Hubble volume, and $\beta R$ is the mean length of a loop with radius $R$. Loops with radius smaller than $\gamma G\mu t$ live for less than a Hubble expansion

*hao.jiao@mail.mcgill.ca
†rhb@physics.mcgill.ca
‡alexandre.refregier@phys.ethz.ch

[1]In this work, we use the natural units with $c = k_B = \hbar = 1$, so the Hubble radius is $r_H = H^{-1} \sim t$.

 

time and their comoving number density can be taken to be independent of $R$.

The strongest robust bound on the string tension stems from the angular power spectrum of cosmic microwave background (CMB) anisotropies and is $G\mu < 10^{-7}$, which is true for both Nambu-Goto cosmic strings [9] and Abelian Higgs cosmic strings [10]. By looking at signals of long strings in angular maps and making use of dedicated statistics such as wavelets, the bound could be strengthened [11]. Long strings also yield distinctive signals in 21-cm redshift maps [12], and 21-cm surveys which probe the epoch before reionization have the potential to yield comparable bounds [13].

Since strings form nonlinear density fluctuations beginning at the time when they form, string loops will dominate early nonlinear structure formation and could explain the origin of high redshift supermassive black holes [14] (see, e.g., [15] for a review on supermassive black holes). In a previous paper [16], we have computed the halo mass function obtained from a scaling distribution of string loops. As expected, we found that the resulting halo mass function dominates over the corresponding mass function from the standard ΛCDM scenario (based on Gaussian adiabatic primordial fluctuations) at high redshifts. This is illustrated in Fig. 1 which is an updated version[2] of the corresponding figure in [16]. Our previous work [16] indicates that for a string tension in the range $10^{-9} < G\mu < 10^{-8}$, cosmic strings could explain recent JWST results [17] which indicate an overabundance of high redshift galaxies compared to what the standard ΛCDM model predicts. Our ΛCDM curves make use of the Press-Schechter mass function [18] at redshifts greater than or equal to 10, and the Sheth-Tormen mass function [19] at lower redshifts.[3]

In our previous work, we did not consider the interplay between fluctuations seeded by strings and those generated by the ΛCDM perturbations. At high redshifts, this is a reasonable approximation, but as soon as the ΛCDM-induced inhomogeneities become important, this approximation breaks down, and the interplay between the fluctuations seeded by the two sources must be considered. Here, we take a first step towards addressing this challenge. We perform $N$-body simulations of structure formation with both of the effects of string loops and ΛCDM fluctuations included. The bottom line of our study is that the resulting halo mass function closely follows that mass function obtained by adding the mass functions of the individual sources. This result will be useful in analyzing the effects of cosmic string loops in the mildly nonlinear phase of structure formation.

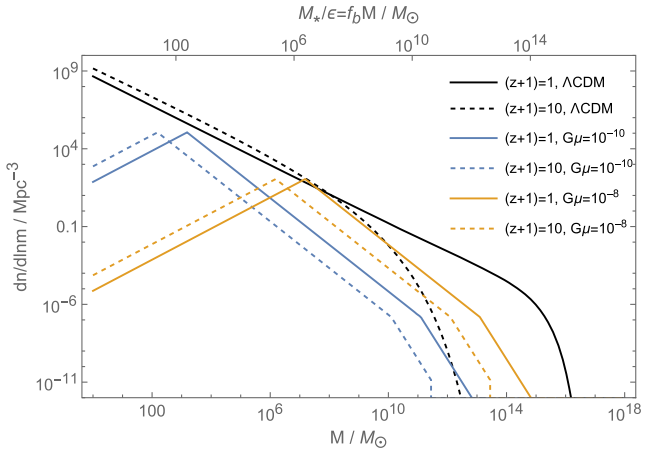


FIG. 1. Comparison of the halo mass function sourced by a scaling distribution of string loops with the corresponding mass function in the ΛCDM model. The halo mass is indicated on the bottom horizontal axis (while the top one indicates the stellar mass as a function of the stellar formation efficiency parameter $\epsilon$ and the baryon fraction $f_b$). The black curves show the halo mass function in the ΛCDM model for redshifts $z+1=1$ (solid curves) and $z+1=10$ (dashed curves). In orange and blue are the corresponding halo mass functions due to strings at the corresponding redshifts. The results for two interesting values of the string tension are shown: $G\mu = 10^{-8}$ in orange and $G\mu = 10^{-10}$ in blue. While the ΛCDM mass function dominates at late times, the effect of the string loops is more important at higher redshifts. The turnover redshift above which the strings dominate depends on $G\mu$. Considering redshifts close to the turnover, we see that the string loops dominate at the higher mass end while the ΛCDM fluctuations are more important for smaller masses. This can be seen by considering the mass functions at redshift $z = 10$ for $G\mu = 10^{-8}$.

## II. NUMERICAL SETUP

Our numerical simulations make use of the Gadget-2 code [21] with ΛCDM initial conditions generated from Planck-normalized Gaussian ΛCDM fluctuations by means of the N-GenIC code [22].[4] The initial conditions for the $N$-body simulations were set at a redshift of $z+1=32$, deep in the region where linear perturbation theory can be trusted. The resulting initial positions and velocities of the particles were then displaced according to the effects which a scaling distribution of cosmic string loops would have, computed in the Zel'dovich approximation [24]. This procedure is discussed in detail in the Appendix.

The Rockstar code [25] is used to identify halos in the output of the simulations. We ran simulations with $N_{\text{particle}} = 256^3$ particles in a box of comoving box size

[2]Compared to the work of [16], we here included an extra factor of 2/5 in the accretion by a string loop of mass, following the prescription in [1].

[3]As shown in [20], the Sheth-Tormen formalism predicts the halo mass function more accurately at low redshifts but overestimates the abundance of halos at redshift $z \gtrsim 10$.

[4]We use the PYTHON package LensTools [23] to read and write Gadget snapshots.

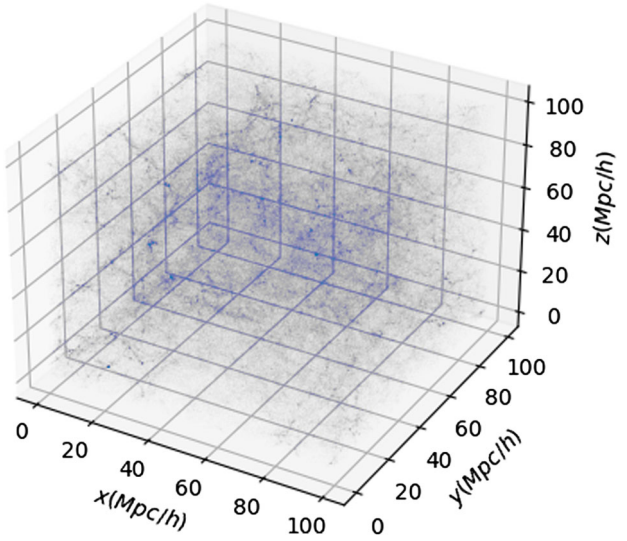


FIG. 2. Distribution of dark matter particles in a pure ΛCDM simulation at redshift $z+1=4$. These particles are illustrated by semitransparent, pale blue points, and overdensities are shown by a deeper shade of blue.

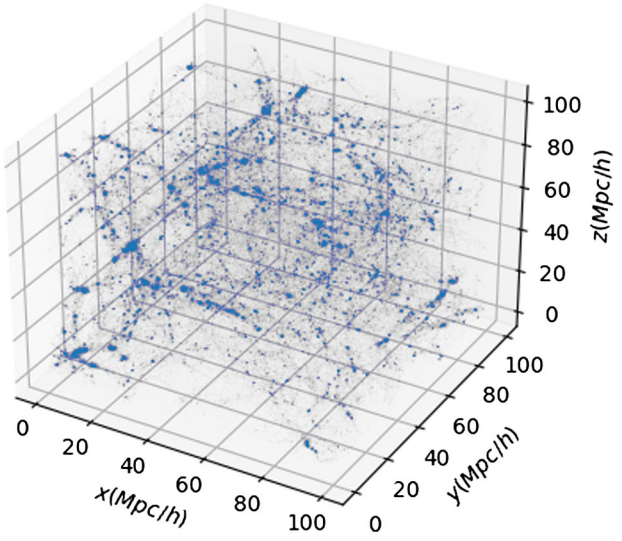


FIG. 3. The distribution of dark matter particles in the same simulation as Fig. 2 at redshift $z+1=1$.

$100h^{-1}$ Mpc, where $h$ is the value of the Hubble constant in units of 100 km/ sec Mpc and we set it to be 0.7 in our simulations.

Note that the falloff of our mass function at the low mass end is due to the fact that because of computational limits, we only consider cosmic string loops with mass greater than $10^{16}(G\mu)M_{\odot}$, which corresponds to a loop radius $R=0.002t_{eq}$, and there are 263 loops in our simulation box.

The following figures show snapshots of our results. Figures 2 and 3 show the distribution of the mass points in a pure ΛCDM simulation at a redshifts of $z+1=4$ and $z+1=1$, respectively, while Figs. 4 and 5 are corresponding to snapshots at the same redshifts if the effects of a scaling distribution of cosmic strings with a large value $G\mu=10^{-7}$ of the string tension are added. Note that the Gaussian seeds were taken to be the same in the simulations with and without the strings. As expected, the effects of cosmic strings are very difficult to be identified by eye at these low redshifts. Only a couple of cosmic string loop-seeded halos can be seen at redshift $z+1=4$, which are indicated by red circles in Fig. 4.

The code was tested in various ways. First, the numerically obtained halo mass function in a pure ΛCDM model was compared to the analytical results obtained using the combination of the Sheth-Tormen [19] and Press-Schechter [18] formalisms. The numerical and analytical results are indeed in good agreement as is shown in Fig. 6.[5] As is apparent, there are no nonlinear halos at high redshifts.

[5]Due to the resolution limit, the numerical mass function at the low-mass end is inaccurate.

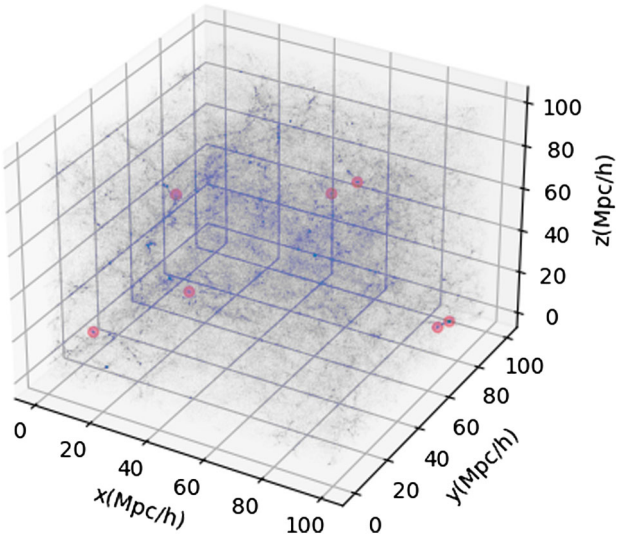


FIG. 4. Distribution of dark matter particles in a simulation which includes both ΛCDM fluctuations (with the same seeds as those in Fig. 2) and cosmic strings with tension $G\mu=10^{-7}$ at redshift $z+1=4$. The red circles mark the position of several prominent loop-seeded halos.

Figure 7 shows the corresponding mass functions in a simulation with only cosmic strings (with tension $G\mu=10^{-7}$). The numerical results are the solid curves, and the analytical curves are given by the dotted lines. First of all, we note that cosmic strings seed large mass nonlinear halos at high redshifts. Second, we note a good agreement between the slopes of the numerical and analytical curves for middle masses. At redshift $(z+1)=16$, the two mass functions almost overlap, while at lower redshifts, the numerical curves are roughly a factor 2 greater than the theoretical ones, due to the fact that the Zel'dovich

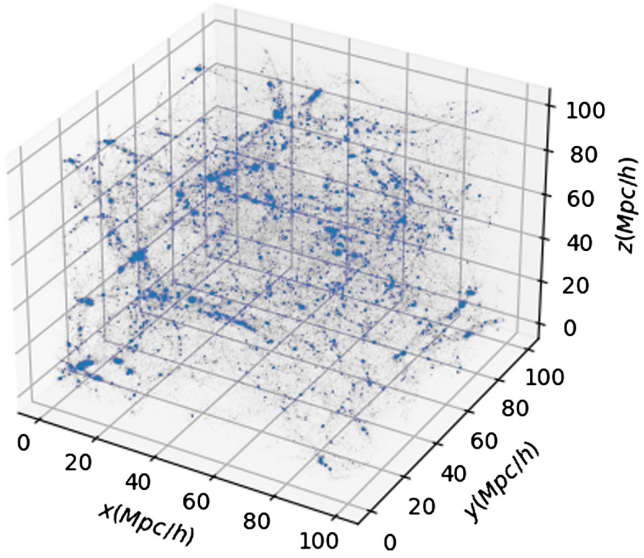


FIG. 5. Distribution of dark matter particles in the simulation of Fig. 4 at redshift $z+1=1$.

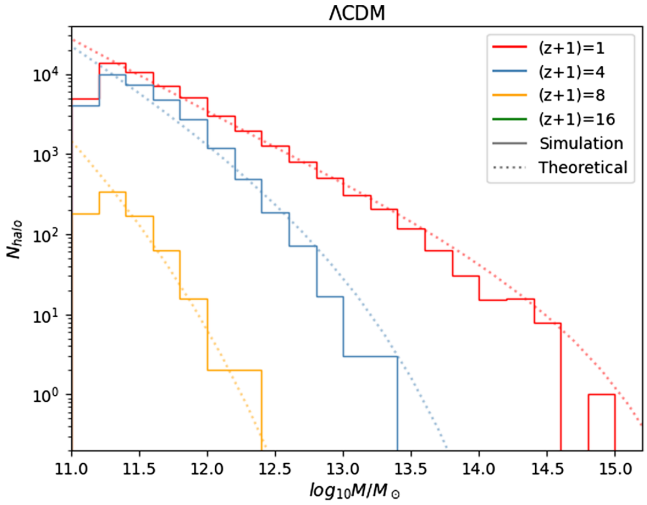


FIG. 6. Comparison between the numerically obtained halo mass function (solid curves) with the analytical approximation (dotted curves) in a pure ΛCDM simulation at two redshifts. The vertical axis gives the number of halos in the mass bin with width $d\lg(M/M_\odot)=0.2$ in the simulation volume. Note that there are too few halos at a redshift $z+1=16$ to be found in the simulation volume, and are therefore not shown.

approximation is only valid for linear perturbations and nonlinear effects will enhance the clustering at low redshifs. Thus, the mass function calculated with the Zel'dovich approximation underpredicts the abundance of loop-seeded halos at redshifts $(z+1)\leq 8$. However, we can find that the evolution of these loop-seeded halos can still be roughly described by the growth factor $M_{\text{loop-seeded}}(t)\propto(z+1)^{-1}$. Therefore, we add a factor 2 to the theoretical cosmic string mass function artificially for $(z+1)\leq 8$ (when nonlinear

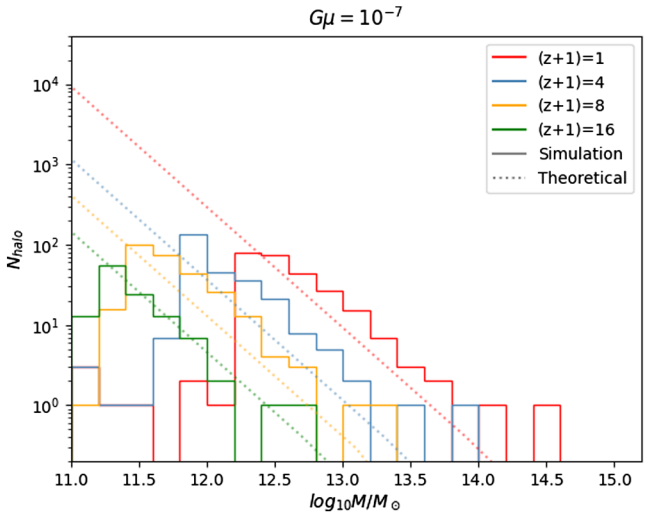


FIG. 7. Comparison between the numerically obtained halo mass function (solid curves) with the analytical approximation (dotted curves) in a pure cosmic string simulation with $G\mu=10^{-7}$. The results at three redshifts are shown. Note that cosmic strings lead to large mass nonlinear halos at high redshifts while the standard ΛCDM model does not.

effects become important) when we study the interplay between loop-seeded overdensities and ΛCDM fluctuations.

The dropoff of the numerical mass functions for small masses results from the cutoff of loops with mass smaller than $10^{16}(G\mu)M_\odot$, which corresponds to loop-seeded halo mass $1.3\times10^{12}(z+1)^{-1}M_\odot$ for $G\mu=10^{-7}$ and is consistent with the lower bound of these numerical curves. The numerical mass function is inaccurate at the highest mass end due to the small number of samples in these mass bins.

Now that we have hopefully persuaded the reader that our code is working correctly, we can turn to the results.

## III. RESULTS

We have performed a series of $N$-body simulations[6] containing both ΛCDM fluctuations and a scaling distribution of string loops with various values of the string tension $G\mu$. The key question we wish to address is how the numerically computed halo mass function compares to the sum of the analytically computed string halo mass function superposed with the analytical ΛCDM mass function obtained by means of the extended Press-Schechter model.

Figure 8 shows the results for simulations with $G\mu=10^{-7}$ at a redshift $(z+1)=6$, a redshift chosen because for the value of $G\mu$ used, the two analytical mass functions cross—the string-induced mass function

[6]We ran 9 simulations with different N-GenIC seeds and different distributions of loops following the number density in (1) and (2) and random spatial distribution to get the average and standard deviation (shaded region in Figs. 8–10) of the halo mass function.

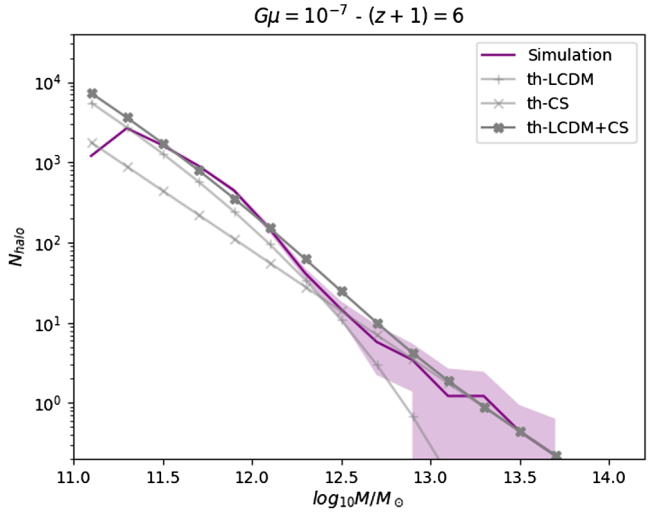


FIG. 8. Mass function in simulations with both cosmic strings ($G\mu = 10^{-7}$) and ΛCDM fluctuations at the redshift $(z+1) = 6$ when the theoretical cosmic string and ΛCDM mass functions cross. The purple line is the average of mass functions in the 9 simulations and the shaded region shows the standard deviation. Gray lines with plus signs, thin crosses and thick crosses are analytical mass functions with only cosmic strings, only ΛCDM fluctuations and both of them, separately. The numerical simulations show that the resulting mass function closely follows the sum of the two theory curves.

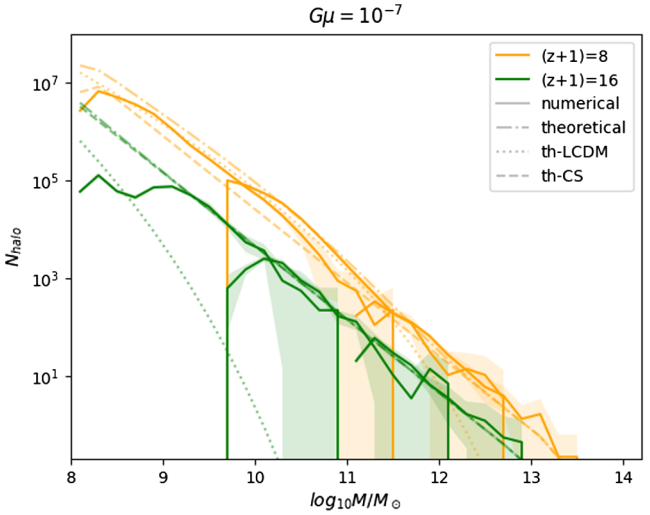


FIG. 9. Mass function in simulations with both cosmic strings ($G\mu = 10^{-7}$) and ΛCDM fluctuations at redshifts $z+1 = 8$ (yellow) and $z+1 = 16$ (green). Here, simulations in three different box sizes were patched together, and thus the envelope of the three numerical curves for each color should be considered. The dotted curves correspond to the ΛCDM theory predictions, the dashed one to the cosmic string predictions, and the dot-dashed curve to the total theory curves (note that these faint curves are also color-coded). The numerically determined halo mass function follows the total theory curve except for small masses, which is due to the mass resolution of these simulations.

(indicated by th-CS) dominating for larger masses while the ΛCDM curve (indicated by th-LCDM) is higher at the low mass end. The results of the numerical analysis are shown in color (with the spread indicating the variance of the results). We see that the results agree well with the theory curve (indicated by th-LCDM+CS) which is the addition of the cosmic string and ΛCDM theory curves.

With the small number of mass points which we have simulated we have a limited mass resolution. To obtain results for a wider range of masses we have patched together simulations (including both strings and ΛCDM fluctuations) in different sized boxes.[7] The resulting mass functions are shown in Figs. 9 and 10, the former for $G\mu = 10^{-7}$ and the latter for $G\mu = 10^{-8}$. Note that the error bars in each simulation are large at the high mass end. Hence, when we combine the three simulations, the error bars are large at values of the mass at the transition points between the low and high mass ends of the different simulations.

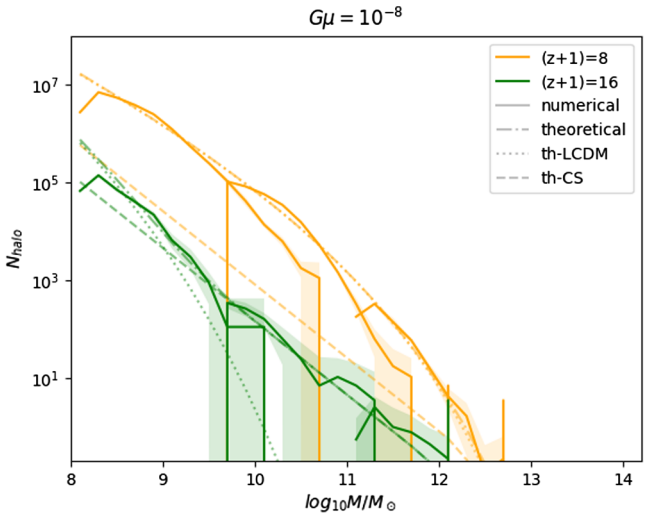


FIG. 10. Same as Fig. 9 but for $G\mu = 10^{-8}$.

## IV. DISCUSSION

We have studied early nonlinear structure formation for a model in which, in addition to the standard Gaussian ΛCDM fluctuations, there is a scaling distribution of cosmic string loops. We find that the resulting numerically computed halo mass function matches well a theoretical curve which is the superposition of the string loop-induced

[7]Here we consider three different box sizes—$10^2 h^{-1}$ Mpc, $10^{3/2} h^{-1}$ Mpc, and $10 h^{-1}$ Mpc, and run 9 simulations with $N_{\rm particle} = 256^3$ particles for each of them. The cutoff mass of cosmic string loops in the different simulations was chosen to keep the numbers of loops in the simulations the same. In the simulation in a box of size $10^{3/2} h^{-1}$ Mpc simulation, the cutoff mass is $10^{15}(G\mu)M_\odot$ while it is $M_{\rm cutoff} = 10^{14}(G\mu)M_\odot$ for box size equal to $10 h^{-1}$ Mpc. Therefore, the masses of loops in smaller boxes are systematically smaller, leading to loop-seeded halos in lower mass range.

halo mass function and the usual ΛCDM halo mass function at high redshifts, while for $(1+z) \lesssim 10$, the loop-induced halo mass should be increased by a factor two according to the $N$-body simulations. This result will allow us to more reliably compute the effects of cosmic strings on early structure formation in the mildly nonlinear region, in particular in the redshift range of reionization.

Our analysis demonstrates that ΛCDM fluctuations do not interfere with the role that cosmic string loops could play in early structure formation, e.g., in generating the seeds for high redshift supermassive black holes [14] and high redshift galaxies [16]. The string tensions we have explored are below the current robust upper bound, but higher than the value of $G\mu \sim 10^{-10.5}$ which is preferred if cosmic strings are to explain the recently detected [26] gravitational wave signal in millisecond pulsar timing arrays (PTAs) [27] (see also [28] for earlier work). In this context, it is important to take into account that it is smaller loops which dominate the PTA signal while it is larger loops which are relevant for supermassive black hole formation, and for explaining early galaxy formation. The small loop distribution is more affected by the unknown physics that goes into establishing a formula for the loop distribution function such as the "one-scale model" than the distribution of larger loops. Hence, cosmic strings with tension $G\mu > 10^{-10.5}$ could well be consistent with the PTA constraints.

In this work, we consider Nambu-Goto cosmic strings with the "one-scale model" of the string loop distribution given by (1) and (2), which is consistent with the results from the more recent Nambu-Goto simulations of [8], in particular with the BOS model (the fifth item in [8]) which is model A in the recent article by the LIGO-VirgoKAGRA collaboration [29]). The reader should be aware that there remain uncertainties in the string loop distribution. Due to the very large hierarchy of scales between cosmological length scales and the width of a string, there are serious obstacles toward deriving robust predictions. In fact, some field theory simulations [30] (which resolve the string width) indicate that loops may decay predominantly into particles, thus greatly suppressing the loop density. But these field theory simulations do not have access to cosmological scales. Nambu-Goto simulations, on the other hand, cannot resolve processes like loop intersections and rely on extra assumptions. Hence, different cosmic string models can generate different loop distributions. However, these uncertainties do not effect our main conclusions, namely that cosmic string loops will dominate the high redshift halo mass function, and that the existence of ΛCDM fluctuations does not systematically influence the evolution of loop-seeded halos, and thus, the mass function derived from the corresponding loop distribution is still reliable at low redshifts with small modifications due to nonlinear effects.

## ACKNOWLEDGMENTS

R. B. wishes to thank the Pauli Center and the Institutes of Theoretical Physics and of Particle- and Astrophysics of the ETH for hospitality. The research of R. B. and H. J. at McGill is supported in part by funds from NSERC and from the Canada Research Chair program. H. J. wishes to thank Juan Gallego, Matteo Puel, Pascale Berner, Pascal Hitz and Uwe Schmitt for help with the numerics.

## APPENDIX: ACCRETION ONTO A STRING LOOP

Here we explain how we modify the initial conditions for our Gadget-2 simulations to take into account the effect of a scaling distribution of string loops. We start with a distribution of dark matter particles generated from Planck-normalized Gaussian ΛCDM fluctuations obtained from the N-GencIC code. We then consider a distribution of cosmic string loops with a size distribution obtained from the cosmic string scaling solution described in the Introduction section, and with uncorrelated loop positions.

We use the Zel'dovich approximation [24] to calculate the displacement and velocity of dark matter particles due to a loop which are used in the initial conditions for the Gadget-2 simulation. For each dark matter particle in the simulation, we consider the change in position and velocity induced by string loops, treating the effects of each loop independently.

The Zel'dovich approximation considers the evolution of mass shells surrounding the string loops. The Newtonian gravity effect of the loop causes the Hubble expansion of the shell to slow down, and eventually the shell "turns around", i.e. the physical distance of the shell from the loops stops increasing. The Zel'dovich approximation is only valid before the particles turn around. After turn-around, we assume that the particles virialize before the initial time of the numerical simulation.

It is justified to view the cosmic string loop as a point source since the separation of the particles in our simulation is large compared to the loop size (note that the impact of the finite size of oscillating loops is studied in [31]). Therefore, the accretion onto a loop is spherically symmetric and thus we only need to calculate the radial component of the coordinates and velocities of the particles relative to the center of the loop.

In the Zel'dovich approximation, we consider the physical distance $h(q,t)$ of a shell with initial comoving distance $q$ from the loop, and denote by $\psi(q,t)$ the comoving displacement of the shell as a consequence of the gravitational attraction. We consider only accretion in the matter-dominated era and hence take the scale factor to be $a(t) = (t/t_0)^{2/3}$. The relation between $h$ and $\psi$ is

$$h(q,t) = a(t)(q - \psi(q,t)). \tag{A1}$$

The dynamics of the test particle is described by Newtonian gravity, i.e.

$$\ddot{h} = -\frac{\partial \Phi}{\partial h}, \tag{A2}$$

where the gravitational potential $\Phi$ is determined by the Poisson equation

$$\nabla^2 \Phi = 4\pi G(\rho_{bg} + \rho_{\rm string}), \tag{A3}$$

where $\rho_{\rm string} = M_{\rm loop}\delta(\mathbf{x})$ is the energy density due to the string loop (taken to be at the origin of the coordinate system). These two equations can be combined to yield the following equation of motion for $\psi$:

$$\ddot{\psi} + \frac{4}{3}t^{-1}\dot{\psi} - \frac{2}{3}t^{-2}\psi = \frac{GM_{\rm loop}}{q^2}\left(\frac{t_0}{t}\right)^2, \tag{A4}$$

where $M_{\rm loop} = \beta\mu R$ is the total mass of the string loop with radius $R$. With initial conditions $\psi(t_i) = \dot{\psi}(t_i) = 0$ the solution is

$$\psi(q,t) = \frac{3}{2}\frac{GM_{\rm loop}t_0^2}{q^2}\left[-1 + \frac{3}{5}\left(\frac{t}{t_i}\right)^{2/3} + \frac{2}{5}\left(\frac{t_i}{t}\right)\right], \tag{A5}$$

Here, $t_i$ is the time that the loop begins to accrete, which is $t_{eq}$ for loops formed in the radiation phase, while for loop formed in the matter phase we have $t_i = \alpha R/\beta$, which is the formation time of this loop. The comoving velocity of the test particles is

$$\dot{\psi}(t) = \frac{3}{5}\frac{GM_{\rm loop}t_0^2}{q^2 t_i}\left[\left(\frac{t_i}{t}\right)^{1/3} - \left(\frac{t_i}{t}\right)^2\right]. \tag{A6}$$

We can calculate the radius of the turnaround shell by solving the equation

$$\dot{h}(q_{nl}(t), t) = 0, \tag{A7}$$

which yields

$$q_{nl} \simeq \left(\frac{9}{5}GMt_0^2\right)^{1/3}\left(\frac{t}{t_i}\right)^{2/9}. \tag{A8}$$

For particles with distance $q > q_{nl}(t)$ (where $t$ is taken to be the initial time of the $N$-body simulation) from a loop, we model the effect of the string loop by adding displacements and velocities toward the loop given by (A5) and (A6) to their original coordinates and velocities.

For particles with distance $q < q_{nl}(t)$ from one of the loops, we assume that the particle has virialized in the halo created by the loop. This implies that the physical distance of the particle from the loop will be half of the physical turnaround radius.

The physical distance of the particle at the time $t_{ta}$ of turnaround is

$$h(t_{ta}) = a(t_{ta})(q - \psi(t_{ta})) = \frac{1}{2}a(t_{ta})q. \tag{A9}$$

Thus, the physical and comoving distances of the particles from the loop will be given by

$$h_{\rm vir}(q) = \frac{1}{2}h(t_{ta}, q) = \frac{1}{4}a(t_{ta})q, \tag{A10}$$

$$r^c_{\rm vir}(q,z) = \frac{1}{a(t)}h_{\rm vir}(q) = \frac{1}{4}\frac{a(t_{ta})}{a(t)}q = \frac{1}{4}\frac{z}{z_{ta}}q, \tag{A11}$$

where $z_{ta}$ is the redshift corresponding to the turnaround time $t_{ta}$. This redshift can be determined by solving $\dot{h}(q, t_{ta}(q)) = 0$ and yields

$$\left(\frac{z_i}{z_{ta}}\right) \simeq \frac{5q^3}{9GM_{\rm loop}t_0^2}. \tag{A12}$$

Thus, we obtain

$$r^c_{\rm vir}(z) \equiv q - \psi(z) \simeq \frac{5}{36}\frac{q^4}{GM_{\rm loop}t_0^2}\frac{z}{z_i} \tag{A13}$$

The velocity of test particles can be computed by requiring the physical height of the particle to be constant. This leads to a comoving velocity of a virialized particle toward the string loop of magnitude

$$\dot{h}_{\rm vir} = \dot{a}r^c_{\rm vir} + a\dot{r}^c_{\rm vir} = 0 \tag{A14}$$

which implies

$$\dot{\psi} = \dot{r}^c_{\rm vir} = Hr^c_{\rm vir} = \frac{2}{3t}r^c_{\rm vir}. \tag{A15}$$

Note that for dark matter particles which are within the virialized radius of a particular loop, no effects from other loops are taken into account.

[1] A. Vilenkin and E. P. S. Shellard, *Cosmic Strings and Other Topological Defects* (Cambridge University Press, Cambridge, England, 2000).

[2] M. B. Hindmarsh and T. W. B. Kibble, Cosmic strings, Rep. Prog. Phys. **58**, 477 (1995).

[3] R. H. Brandenberger, Topological defects and structure formation, Int. J. Mod. Phys. A **09**, 2117 (1994).

[4] T. W. B. Kibble, Phase transitions in the early universe, Acta Phys. Pol. B **13**, 723 (1982), https://inspirehep.net/literature/170526; Some implications of a cosmological phase transition, Phys. Rep. **67**, 183 (1980).

[5] T. Vachaspati and A. Vilenkin, Gravitational radiation from cosmic strings, Phys. Rev. D **31**, 3052 (1985).

[6] M. Hindmarsh, J. Lizarraga, J. Urrestilla, D. Daverio, and M. Kunz, Scaling from gauge and scalar radiation in Abelian Higgs string networks, Phys. Rev. D **96**, 023525 (2017).

[7] E. J. Copeland, T. W. B. Kibble, and D. Austin, Scaling solutions in cosmic string networks, Phys. Rev. D **45**, R1000 (1992); L. Perivolaropoulos, COBE versus cosmic strings: An analytical model, Phys. Lett. B **298**, 305 (1993); D. Austin, E. J. Copeland, and T. W. B. Kibble, Evolution of cosmic string configurations, Phys. Rev. D **48**, 5594 (1993).

[8] C. Ringeval, M. Sakellariadou, and F. Bouchet, Cosmological evolution of cosmic string loops, J. Cosmol. Astropart. Phys. 02 (2007) 023; V. Vanchurin, K. D. Olum, and A. Vilenkin, Scaling of cosmic string loops, Phys. Rev. D **74**, 063527 (2006); L. Lorenz, C. Ringeval, and M. Sakellariadou, Cosmic string loop distribution on all length scales and at any redshift, J. Cosmol. Astropart. Phys. 10 (2010) 003; J. J. Blanco-Pillado, K. D. Olum, and B. Shlaer, Large parallel cosmic string simulations: New results on loop production, Phys. Rev. D **83**, 083514 (2011); The number of cosmic string loops, Phys. Rev. D **89**, 023512 (2014); P. Auclair, C. Ringeval, M. Sakellariadou, and D. Steer, Cosmic string loop production functions, J. Cosmol. Astropart. Phys. 06 (2019) 015; J. J. Blanco-Pillado and K. D. Olum, Direct determination of cosmic string loop density from simulations, Phys. Rev. D **101**, 103018 (2020).

[9] T. Charnock, A. Avgoustidis, E. J. Copeland, and A. Moss, CMB constraints on cosmic strings and superstrings, Phys. Rev. D **93**, 123503 (2016); C. Dvorkin, M. Wyman, and W. Hu, Cosmic string constraints from WMAP and the South Pole Telescope, Phys. Rev. D **84**, 123519 (2011); P. A. R. Ade *et al.* (Planck Collaboration), Planck 2013 results. XXV. Searches for cosmic strings and other topological defects, Astron. Astrophys. **571**, A25 (2014).

[10] J. Lizarraga, J. Urrestilla, D. Daverio, M. Hindmarsh, and M. Kunz, New CMB constraints for Abelian Higgs cosmic strings, J. Cosmol. Astropart. Phys. 10 (2016) 042.

[11] L. Hergt, A. Amara, R. Brandenberger, T. Kacprzak, and A. Refregier, Searching for cosmic strings in CMB anisotropy maps using wavelets and curvelets, J. Cosmol. Astropart. Phys. 06 (2017) 004.

[12] R. H. Brandenberger, R. J. Danos, O. F. Hernandez, and G. P. Holder, The 21 cm signature of cosmic string wakes, J. Cosmol. Astropart. Phys. 12 (2010) 028.

[13] D. Maibach, R. Brandenberger, D. Crichton, and A. Refregier, Extracting the signal of cosmic string wakes from 21-cm observations, Phys. Rev. D **104**, 123535 (2021).

[14] S. F. Bramberger, R. H. Brandenberger, P. Jreidini, and J. Quintin, Cosmic string loops as the seeds of super-massive black holes, J. Cosmol. Astropart. Phys. 06 (2015) 007; R. Brandenberger, B. Cyr, and H. Jiao, Intermediate mass black hole seeds from cosmic string loops, Phys. Rev. D **104**, 123501 (2021); B. Cyr, H. Jiao, and R. Brandenberger, Massive black holes at high redshifts from superconducting cosmic strings, Mon. Not. R. Astron. Soc. **517**, 2221 (2022).

[15] M. Volonteri, Formation of supermassive black holes, Astron. Astrophys. Rev. **18**, 279 (2010).

[16] H. Jiao, R. Brandenberger, and A. Refregier, Early structure formation from cosmic string loops in light of early JWST observations, Phys. Rev. D **108**, 043510 (2023).

[17] Y. Harikane, M. Ouchi, M. Oguri, Y. Ono, K. Nakajima, Y. Isobe, H. Umeda, K. Mawatari, and Y. Zhang, A comprehensive study on galaxies at $z \sim 9$–16 found in the early JWST data: UV luminosity functions and cosmic star-formation history at the pre-reionization epoch, Astrophys. J. Suppl. Ser. **265**, 5 (2023); R. Naidu *et al.*, Schrodinger's galaxy candidate: Puzzlingly luminous at $z \simeq 17$, or dusty / quenched at $z \simeq 5$? arXiv:2208.02794; M. Boylan-Kolchin, Stress testing ΛCDM with high-redshift galaxy candidates, arXiv:2208.01611; A. Ferrara, A. Pallottini, and P. Dayal, On the stunning abundance of super-early, massive galaxies revealed by JWST, arXiv:2208.00720; C. C. Lovell, I. Harrison, Y. Harikane, S. Tacchella, and S. M. Wilkins, Extreme value statistics of the halo and stellar mass distributions at high redshift: Are JWST results in tension with ΛCDM?, Mon. Not. R. Astron. Soc. **518**, 2511 (2022); I. Labbe *et al.*, A population of red candidate massive galaxies 600 Myr after the Big Bang, Nature (London) **616**, 266 (2023); Revealing galaxy candidates out to $z \sim 16$ with JWST observations of the lensing cluster SMACS0723, Mon. Not. R. Astron. Soc. **519**, 1201 (2022); C. Donan *et al.*, The evolution of the galaxy UV luminosity function at redshifts $z \sim 8$–15 from deep JWST and ground-based near-infrared imaging, Mon. Not. R. Astron. Soc. **518**, 6011 (2022); S. Finkelstein *et al.*, A long time ago in a galaxy far, far away: A candidate $z \sim 12$ galaxy in early JWST CEERS imaging, arXiv:2207.12474.

[18] W. H. Press and P. Schechter, Formation of galaxies and clusters of galaxies by self-similar gravitational condensation, Astrophys. J. **187**, 425 (1974).

[19] R. K. Sheth and G. Tormen, Large-scale bias and the peak background split, Mon. Not. R. Astron. Soc. **308**, 119 (1999); R. K. Sheth, H. J. Mo, and G. Tormen, Ellipsoidal collapse and an improved model for the number and spatial distribution of dark matter haloes, Mon. Not. R. Astron. Soc. **323**, 1 (2001); R. K. Sheth and G. Tormen, An excursion set model of hierarchical clustering: Ellipsoidal collapse and the moving barrier, Mon. Not. R. Astron. Soc. **329**, 61 (2002).

[20] A. Jenkins, C. S. Frenk, S. D. M. White, J. M. Colberg, S. Cole, A. E. Evrard, H. M. P. Couchman, and N. Yoshida, The mass function of dark matter haloes, Mon. Not. R. Astron. Soc. **321**, 372 (2001); D. Reed, J. Gardner, T. Quinn, J. Stadel, M. Fardal, G. Lake, and F. Governato, Evolution of the mass function of dark matter haloes, Mon. Not. R. Astron. Soc. **346**, 565 (2003); A. A. Klypin, S. Trujillo-Gomez, and J. Primack, Dark matter halos in the

standard cosmological model: Results from the Bolshoi simulation, Astrophys. J. **740**, 102 (2011).

[21] V. Springel, The cosmological simulation code Gadget-2, Mon. Not. R. Astron. Soc. **364**, 1105 (2005); V. Springel, N. Yoshida, and S. D. M. White, Probing the stellar surface of HD 209458 from multicolor transit observations, New Astron. **6**, 51 (2001); Gadget: A code for collisionless and gasdynamical cosmological simulations, New Astron. **6**, 79 (2001).

[22] V. Springel *et al.*, Simulations of the formation, evolution and clustering of galaxies and quasars, Nature (London) **435**, 629 (2005); R. E. Angulo, V. Springel, S. D. M. White, A. Jenkins, C. M. Baugh, and C. S. Frenk, Scaling relations for galaxy clusters in the Millennium-XXL simulation, Mon. Not. R. Astron. Soc. **426**, 2046 (2012).

[23] A. Petri, Mocking the weak lensing universe: The LensTools PYTHON computing package, Astron. Comput. **17**, 73 (2016).

[24] Y. B. Zeldovich, Gravitational instability: An approximate theory for large density perturbations, Astron. Astrophys. **5**, 84 (1970), https://inspirehep.net/literature/55133.

[25] P. S. Behroozi, R. H. Wechsler, and H. Y. Wu, The rockstar phase-space temporal halo finder and the velocity offsets of cluster cores, Astrophys. J. **762**, 109 (2012).

[26] G. Agazie *et al.* (NANOGrav Collaboration), The NANOGrav 15 yr data set: Evidence for a gravitational-wave background, Astrophys. J. Lett. **951**, L8 (2023); J. Antoniadis *et al.* (EPTA and InPTA Collaborations), The second data release from the European Pulsar Timing Array—III. Search for gravitational wave signals, Astron. Astrophys. **678**, A50 (2023); D. J. Reardon, A. Zic, R. M. Shannon, G. B. Hobbs, M. Bailes, V. Di Marco, A. Kapur, A. F. Rogers, E. Thrane, J. Askew *et al.*, Search for an isotropic gravitational-wave background with the Parkes Pulsar Timing Array, Astrophys. J. Lett. **951**, L6 (2023); H. Xu, S. Chen, Y. Guo, J. Jiang, B. Wang, J. Xu, Z. Xue, R. N. Caballero, J. Yuan, Y. Xu *et al.*, Searching for the nano-hertz stochastic gravitational wave background with the Chinese Pulsar Timing Array data release I, Res. Astron. Astrophys. **23**, 075024 (2023).

[27] A. Afzal *et al.* (NANOGrav Collaborations), The NANOGrav 15 yr data set: Search for signals from new physics, Astrophys. J. Lett. **951**, L11 (2023).

[28] J. J. Blanco-Pillado, K. D. Olum, and X. Siemens, New limits on cosmic strings from gravitational wave observation, Phys. Lett. B **778**, 392 (2018); Z. Arzoumanian *et al.* (NANOGRAV Collaboration), The NANOGrav 11-year data set: Pulsar-timing constraints on the stochastic gravitational-wave background, Astrophys. J. **859**, 47 (2018).

[29] R. Abbott *et al.* (LIGO Scientific, Virgo, KAGRA Collaborations), Constraints on cosmic strings using data from the third Advanced LIGO-Virgo observing run, Phys. Rev. Lett. **126**, 241102 (2021).

[30] G. Vincent, N. D. Antunes, and M. Hindmarsh, Numerical simulations of string networks in the Abelian Higgs model, Phys. Rev. Lett. **80**, 2277 (1998); J. N. Moore, E. P. S. Shellard, and C. J. A. P. Martins, On the evolution of Abelian-Higgs string networks, Phys. Rev. D **65**, 023503 (2002).

[31] H. Jiao, B. Cyr, and R. Brandenberger, Accretion onto oscillating cosmic string loops, arXiv:2308.14468.